Isotope Effect on the Isothermal Crystallization Behavior of Isotactic Polypropylene Blends between the Deuterated and Hydrogenated Species

Kummetha Raghunatha Reddy,[†] Kohji Tashiro,*[,†] Takashi Sakurai,[‡] and Noboru Yamaguchi[‡]

Department of Future Industry-oriented Basic Science and Materials, Toyota Technological Institute, Tempaku, Nagoya 468-8511, Japan, and Petrochemicals Research Laboratory, Sumitomo Chemical Co. Ltd., Kitasode, Sodegaura, Chiba 299-0295, Japan

Received November 14, 2008; Revised Manuscript Received December 23, 2008

ABSTRACT: The effect of isotope on the isothermal crystallization behavior has been investigated for a series of isotactic polypropylene blend samples between the hydrogenated and deuterated species by using the thermal analysis technique. The analysis based on the Avrami equation revealed the crystallization rate constant k and Avrami exponent n, which were found to change systematically with the D/H content at the same degree of supercooling, reflecting the cocrystallization phenomenon of these two species. The k value was appreciably higher for the D species than for the H species. Correspondingly, the spherulite size, observed by polarized optical microscope and small-angle light scattering, was found to be larger for the blend with higher H content.

Introduction

Physical properties and morphology of a semicrystalline polymer depend not only on such molecular characteristics as molecular weight, molecular weight distribution, and tacticity but also on such processing conditions as cooling rate from the melt, annealing temperature, etc.[1,2] For a better understanding of factors governing the properties of a polymer, a quantitative clarification of the crystallization mechanism is indispensably important. In particular, it is an essential theme to trace the individual chain behavior during the crystallization process. For this purpose we need to label particular chains to distinguish them from the others. The labeling of chains by the deuterated species is one of the most useful methods.[3−9] The basic principle behind the utilization of deuterated species is the difference in neutron scattering length and vibrational frequency between the deuterated and hydrogenated species. In these experiments, it is assumed in general that the *cocrystallization* occurs between the H and D species in the crystalline lattice. But this assumption is not always correct and depends on the kind of polymer under study. For example, the blends between the hydrogenated and deuterated species of the various types of polyethylene were extensively studied to understand the cocrystallization phenomenon between the H and D species.[3−6,9−20] In the case of blend samples between hydrogenated high-density polyethylene (HDPE) and deuterated HDPE (DHDPE), for example, they show the phase segregation phenomenon when cooled slowly from the melt.[6] On the other hand, an almost perfect cocrystallization phenomenon occurs for the blend samples between DHDPE and hydrogenated linear low-density polyethylene (LLDPE) with about 17 ethyl branches/1000 carbon atoms even when cooled slowly from the melt.[10−16] If the LLDPE sample with lower or higher degree of branching is used, the degree of phase segregation becomes higher. The D/H blend samples showing the perfect cocrystallization phenomenon can be used for the trace of D chains during the crystallization process and also for the clarification of the chain folding mode in the crystallization phenomenon. In fact, the research results based on the blend samples of DHDPE/LLDPE (17 ethyl branching) gave us much useful information concerning the crystallization behaviors of individual polyethylene chains.[16] This type of research to check the perfect cocrystallization phenomenon of the D and H species is quite limited for other kinds of polymers. In other words, many crystallization studies on the D/H blend samples do not have enough well-established experimental guarantees about the cocrystallization phenomenon and therefore about the discussion of the crystallization behavior of individual chains.

In the present study we are challenged to understand the crystallization process of *isotactic* polypropylene (iPP) because it is one of the most industrially important semicrystalline polymers. Many researches were reported extensively about the crystallization phenomenon of iPP for the past five decades by various methods.[21−34] As compared with the other polymers, the crystallization of iPP is more complex when cooled from the melt to ambient temperature because it crystallizes to three different polymorphs at least. In addition to the kinetically favorable α-crystal form, iPP crystallizes also into the β- and γ-forms depending on the crystallization conditions.[35] The blend samples of iPP between the H and D species are expected to be useful for the study of crystallization behavior of iPP with such quite complicated aggregation state. Ballard et al. reported small-angle neutron scattering data by utilizing such blend sample between the H and D species of iPP. But they did not discuss the cocrystallization phenomenon itself between these two species.[36−38]

In the previous paper we established the cocrystallization phenomenon between the H and D species of iPP successfully by means of DSC, WAXD, and IR spectral measurements.[39] As shown in Figure 1, the crystallization temperature measured in the DSC thermogram shifts continuously toward the higher temperature side with an increase in the H content. In order to understand the mechanism of the cocrystallization phenomenon, we need to know the crystallization behaviors of a series of these blend samples. In the present paper we report the crystallization kinetics during the isothermal crystallization process for a series of iPP D/H blend samples by the thermal analysis. The thus-obtained data were interpreted on the basis of Avrami equation, from which the various parameters concerning the crystallization kinetics were evaluated and compared among all the members of the D/H blends. At the same time the polarized optical microscopic observation was

* To whom correspondence should be addressed.
[†] Toyota Technological Institute.
[‡] Sumitomo Chemical Co. Ltd.

10.1021/ma802568c CCC: $40.75
Published on Web 02/04/2009

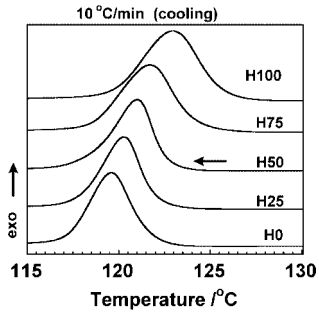

Figure 1. H content dependence of the crystallization point measured for the melt-crystallized iPP blend samples.

Table 1. Characterization of iPP Samples

sample	M_w	M_w/M_n
hydrogenated iPP	160K	3.0
deuterated iPP	200K	2.5

also made for comparing the difference in the morphology among them. The detailed investigation of the isotope effect on the crystallization phenomenon of iPP is indispensable for the trace of a single D chain embedded in the H chain matrix using the neutron method and for the interpretation of cocrystallization mechanism of iPP D/H blend samples.

Experimental Section

Samples. The deuterated and hydrogenated iPP samples were prepared with a metallocene catalyst system. The molecular weights of the polymers were determined by high-temperature gel permeation chromatography with *o*-dichlorobenzene as an eluent. Table 1 shows the characterization of these samples. The molecular weight distributions of the samples used are not very sharp. The experimental analysis would contain some ambiguity about the crystallization rate and so on, but we would proceed the discussion by taking this point into consideration.

The D/H blend samples with molar ratios 0:100, 25:75, 50:50, 75:25, and 100:0 were prepared by dissolving these two components in boiling *p*-xylene at a concentration of 2 wt % followed by precipitation into methanol. The precipitated samples were dried in a vacuum oven at 100 °C and cooled slowly to the room temperature. The thus-obtained blend samples are named here as H*n* where $n = 0-100$ (for example, H75 is the blend sample of H75/D25 mol %).

The DSC thermograms were measured using a differential scanning calorimeter TA DSC Q1000 under a nitrogen gas atmosphere. The temperature scale was calibrated using indium as a standard. The thermal program used in the isothermal crystallization process is shown in Figure 2. The sample was heated to 200 °C at 5 °C/min rate and was kept there for 5 min followed by

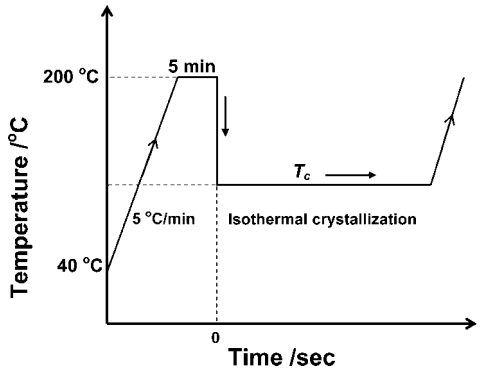

Figure 2. Schematic illustration of the thermal program used in the DSC measurement of the isothermal crystallization process of a series of iPP D/H blend samples.

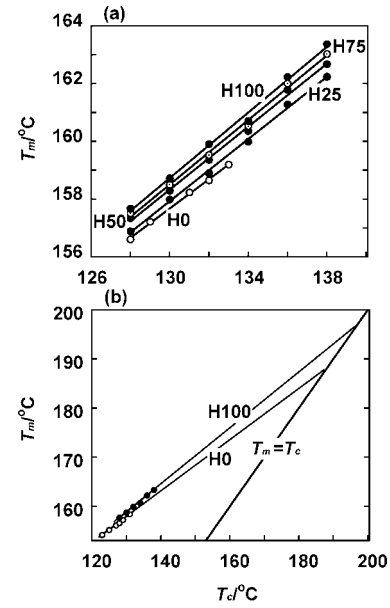

Figure 3. (a) Melting points measured for a series of iPP H/D blend samples crystallized at the temperature T_c. (b) Hoffman−Weeks plots to evaluate the equilibrium melting temperatures, where only the two cases of H0 and H100 samples are shown as examples.

rapid cooling to a predetermined crystallization temperature (T_c). The exothermic peak was recorded as a function of time. After the completion of crystallization the sample was heated up to the melting point to observe the effect of T_c on the melting behavior at 5 °C/min rate.

The wide-angle X-ray diffraction (WAXD) profiles were measured using a Rigaku RINT-TTR III diffractometer. The incident X-ray beam was a graphite-monochromatized Cu Kα radiation ($\lambda = 1.54$ Å). The X-ray diffraction profiles were measured in the 2θ range of 5°−30°, during which the DSC was measured simultaneously at a scanning rate 2 °C/min.

Small-angle light scattering patterns (SALS) were measured for the samples which were isothermally crystallized at T_c. The SALS patterns were measured at room temperature using a DYNA-3000, Otsuka Electronics, Japan, with CCD camera as a 2D detector. A polarized beam from He−Ne laser ($\lambda = 6348$ Å) was incident onto the sample, and the HV patterns were taken using an analyzer. The spherulite radius was calculated by using[40,41]

$$R = 1.025\lambda/[\pi n \sin(\theta_m/2)] \quad (1)$$

where R is an average spherulite radius, λ is a wavelength of the incident light in the air, θ_m is a scattering angle at maximum intensity, and n is a refractive index of the sample (1.5030).[42]

Results and Discussion

Estimation of Equilibrium Melting Point. In order to investigate the crystallization kinetics, we need to know the equilibrium melting points ($T°_m$) of individual blend samples. Figure 3a shows the observed melting points plotted against the crystallization temperature T_c for all the members of D/H blends. The Hoffman−Weeks plots were made to estimate the equilibrium melting point as shown in Figure 3b for the cases of H0 and H100 samples as examples.[43]

$$T_m = \beta T_c + (1 - \beta)T°_m \quad (2\text{-}1)$$

$$T_m = T_c \quad (2\text{-}2)$$

where β represents a stability parameter that depends on the size and perfection of the crystallites. The cross point of two linear lines given in eqs 2-1 and 2-2 should give the $T°_m$ as

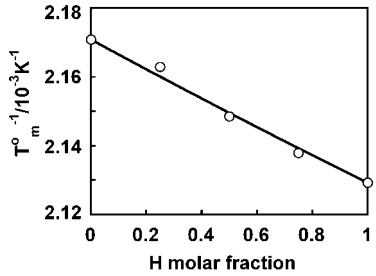

Figure 4. H content dependence of an equilibrium melting point T°_m. A solid line is the curve fitted to the observed data by using an adjustable parameter $T^{\circ}_{mhd} = 465.7$ K $= 192.5$ °C.

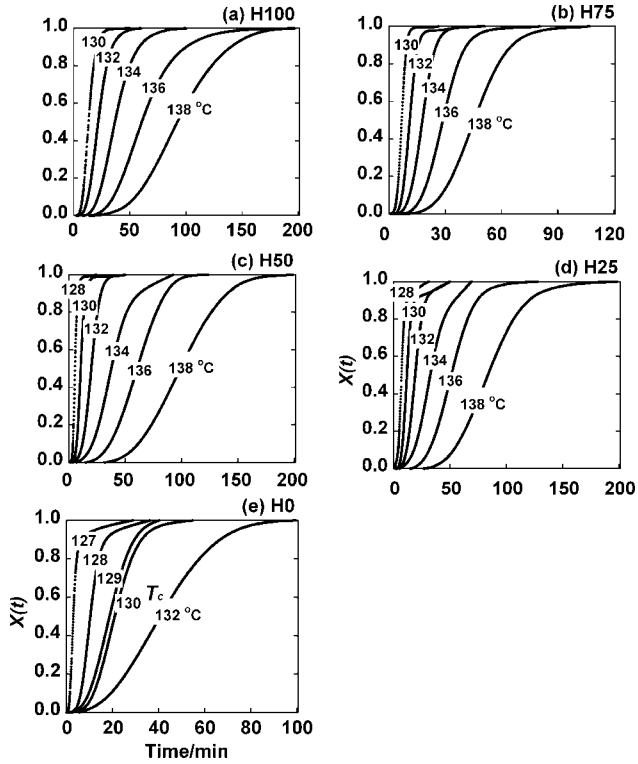

Figure 5. Time dependence of the normalized crystallinity during the isothermal crystallization process measured for a series of H/D iPP blend samples: (a) H100, (b) H75, (c) H50, (d) H25, and (e) H0. In some graphs the data points were picked out for a proper time interval to show the observed points clearly.

shown in Figure 3b. The T°_m of pure H-iPP is 196.5 °C. The T°_m are 194.6, 192.3, 189.2, and 187.5 °C for H75, H50, H25, and H0, respectively. Philiphs et al. measured the T°_m of H100 and H0 samples which were 185 and 177 °C, respectively.[44] But they did not give any information about the characterization of H and D samples. Judging from the relatively high melting points their samples might have been synthesized using a Ziegler−Natta catalyst, but this is only a speculation. In our cases both of H and D species were synthesized using a metallocene catalyst. This catalyst gives in general the relatively lower melting points than Ziegler−Natta catalyst because the former gives a little lower isotacticity.

The thus-evaluated T°_m changes systematically for a series of H/D blend samples as shown in Figure 4. These data points can be fitted reasonably on the basis of the thermodynamic equation derived for the interpretation of isotope effect on the melting point of D/H blend samples which can be cocrystallized so that the D and H chain stems are coexistent statistically randomly within a common lattice.

$$1/T^{\circ}_m = X^2/T^{\circ}_m(\mathrm{H}) + (1 - X)^2/T^{\circ}_m(\mathrm{D}) + 2X(1 - X)/T^{\circ}_{mhd} \quad (3)$$

The solid line shown in Figure 4 is the thus-obtained curve by controlling the adjustable parameter $T^{\circ}_{mhd} = 465.7$ K $= 192.5$ °C.

Isothermal Crystallization. Figure 5 shows the evolution process of the normalized crystallinity estimated for a series of blend samples in the isothermal crystallization process. As the T_c was increased, the crystallization occurred more slowly for each case. These data were analyzed on the basis of the Avrami equation[45−47]

$$1 - X(t) = \exp[-(kt)^n] \quad (4)$$

where $X(t)$ is a normalized crystallinity at a time t, k is a rate constant, and n is an Avrami index. Figure 6 shows the plots of a double logarithm of $X(t)$ against logarithm of time, from which the k and n values were evaluated as listed in Table 2. The n of H100 is between 3 and 4, consistent with the values reported in the literature.[48−50] The n value changes depending on the D/H ratio. In Figure 7 the n and k values are compared among the blend samples crystallized at almost the same degree of supercooling ($\Delta T = T^{\circ}_m - T_c$). The n is related to the dimension of the crystal growth. If the crystallization is assumed to occur homogeneously, $n = 2$ suggests a rodlike growth from sporadically generated nuclei. If the crystallization occurs heterogeneously, $n = 2$ suggests disklike growth from already-existing nuclei or dust particle. $n = 3$ indicates the disklike growth (for homogeneous crystallization) or a spherulite growth (for heterogeneous crystallization). The $n = 4$ suggests the spherulitic growth for the homogeneous crystallization. As seen in Figure 7a, the growth dimension n is dependent on the H content as well as ΔT. For example, the n value is about 4 for H100, indicating the crystal growth of pure H sample is approximately like the 3-dimensional spherulitic growth under the assumption of homogeneous crystallization. As seen in Figure 8, the polarized optical microscopic observation shows the growth of spherulites although the spherulite size becomes smaller for the sample with lower content of H component. The averaged spherulite size was estimated by SALS measurement (Figure 8, $\Delta T = 57$ °C). As seen later (Figure 11), the H100 sample gives large spherulites of 98 μm diameter. For the H0 (pure D) sample the spherulite size is remarkably small, about 8 μm at the same ΔT. As already mentioned, the k value becomes smaller for the sample with higher H content. The slower crystallization of the H100 sample causes the larger spherulites.

The T_c dependence of k allows us to estimate the various parameters related to the crystallization phenomenon. According to Hoffman−Lauritzen nucleation theory,[28] the growth rate k at a crystallization temperature T_c is expressed as

$$k(T_c) = k_0 \exp(-U/[R(T_c - T_\infty)]) \exp(-K_g/[T_c(T^{\circ}_m - T_c)]) \quad (5)$$

where k_0 is a constant, R is the gas constant, and U is the energy for the transport of molecules in the melt, ca. 1500 cal/mol according to the literature.[51] T_∞ is the temperature where all the motions associated with the viscous flow stop and is defined as $T_\infty = T_g - 30$ K ≈ 228 K. Here T_g is the glass transition temperature (258 K),[52] and T°_m is an equilibrium melting point. The nucleation constant K_g is related to the energy required for the formation of nuclei of critical size, defined as $4\sigma\sigma_e T^{\circ}_m/(\Delta H^{\circ}_m k_B)$ and depends on the surface free energy (σ and σ_e) of the crystals and the heat of fusion (ΔH°_m) where b is a iPP chain thickness ≈ 6.26 Å and k_B is the Boltzmann constant.[50] The plot of $[\ln k + U/R(T_c - T_\infty)]$ against $1/[T_c(T^{\circ}_m - T_c)]$

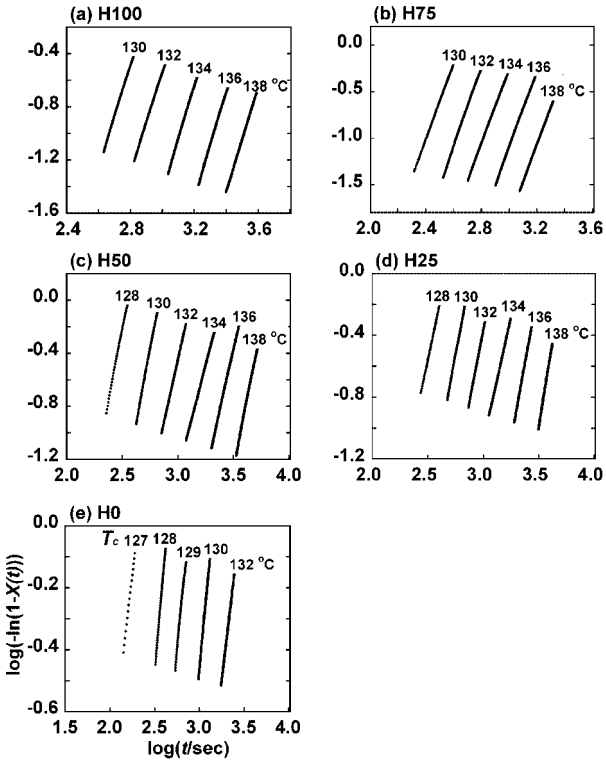

Figure 6. Avrami plots made for the data shown in Figure 4: (a) H100, (b) H75, (c) H50, (d) H25, and (e) H0. The temperature shown in each figure is the isothermal crystallization point.

Table 2. $t_{1/2}$, n, and log k Values for a Series of iPP D/H Blend Samples Crystallized at Various Temperatures

samples	T_c/°C	$t_{1/2}$/s[a]	n	log(k/s^{-1})
H0	127	3.05	2.59	−2.76
	128	10.27	2.61	−2.89
	129	18.66	2.65	−3.05
	130	20.83	2.71	−3.15
	132	40.00	2.65	−3.35
H25	128	6.11	3.38	−2.76
	130	12.22	3.31	−2.98
	132	19.44	3.30	−3.19
	134	32.22	3.27	−3.43
	136	51.11	3.28	−3.62
	138	82.73	3.29	−3.83
H50	128	6.55	3.73	−2.55
	130	10.55	3.74	−2.83
	132	20.00	3.70	−3.02
	134	37.22	3.72	−3.30
	136	61.11	3.73	−3.50
	138	98.88	3.73	−3.70
H75	130	6.66	3.89	−2.64
	132	11.33	3.87	−2.85
	134	17.66	3.85	−3.06
	136	28.66	3.83	−3.27
	138	45.66	3.84	−3.47
H100	130	13.33	3.93	−2.52
	132	22.22	3.73	−2.74
	134	36.66	3.97	−2.96
	136	61.11	3.97	−3.17
	138	92.77	3.94	−3.36

[a] $t_{1/2}$ is a time necessary for the degree of crystallinity to attain at 50%.

should show a straight line, from the intercept and slope of which the k_0 and K_g are obtained, respectively. This type of plot is shown in Figure 9, and the values are tabulated in Table 3 for the several H/D blend samples.

The K_g value for H100 is comparable to the reported values.[53] But there is no clear tendency in the K_g and ln k_0 values for the blend samples (Table 3), suggesting that the isotope chains do not have any influence on the transportability of iPP chains in the melt. The systematic difference in the k itself indicates the typical isotope effect on the crystallization rate.

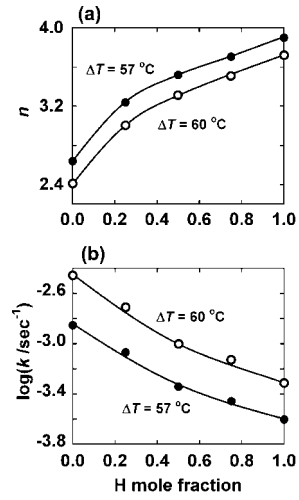

Figure 7. H molar ratio dependence of the Avrami parameters n and k estimated for a series iPP D/H blend samples at the same degree of supercooling (ΔT).

By the way, since the metallocene-catalyzed iPP samples have uniform distribution of defects along the main chain, these defects are prone to the formation of the γ-form along with the α-form when crystallized slowly from the melt.[54−56] In fact, as seen in Figure 10, where the X-ray diffraction profiles are measured for the samples crystallized at the same degree of supercooling (ΔT = 57 °C), all the samples were found to crystallize in the mixture of α- and γ-forms. The γ-fraction was tentatively estimated as $I_\gamma/(I_\gamma + I_\alpha)$, where I_γ and I_α are the integrated intensities of the (117) and (130) X-ray reflection peaks of the γ- and α-modifications, respectively.[57] The crystallite size D_{hkl} along the [hkl] direction is also estimated using Scherrer's equation using a half-width of the X-ray reflection peak of 130 (α-form) or 117 (γ-form) reflection (Figure 10).

$$D_{hkl} = 0.89\lambda/(\beta \cos \theta) \tag{6}$$

where λ is the wavelength of X-rays, β is the line width at half-maximum height of the reflection, and 2θ is a Bragg angle. The thus-obtained structural parameters, i.e., the crystallite size of α- and γ-forms, the γ-form content and the averaged spherulite size are plotted against the H content of the blend, as shown in Figure 11. They change systematically depending on the D/H content. The spherulite size is increasing remarkably for the sample with higher H content close to 100%.

Isotope Effect on Crystallization Rate. In this way the D species of iPP shows appreciably different crystallization behavior from that of the H species. The crystallization occurs faster, and the spherulites are much smaller than the H species. Approximately the crystallization rate of the D/H blend sample is the weighted average of the parameters of the pure H and D species, as shown in Figure 7. As already mentioned, these two species *cocrystallize* when cooled slowly from the melt. We might have the following speculation about the crystallization behavior. Since the H species can crystallize at higher temperature, the cluster of the H species might be created within the matrix of the molten D and H chains. As a result, the molar content of D and H species in the melt might be changed. As the temperature decreases gradually, this isotopic fractionation might proceed furthermore. At some temperature point, the D chains also start to crystallize, and both of the D and H chains

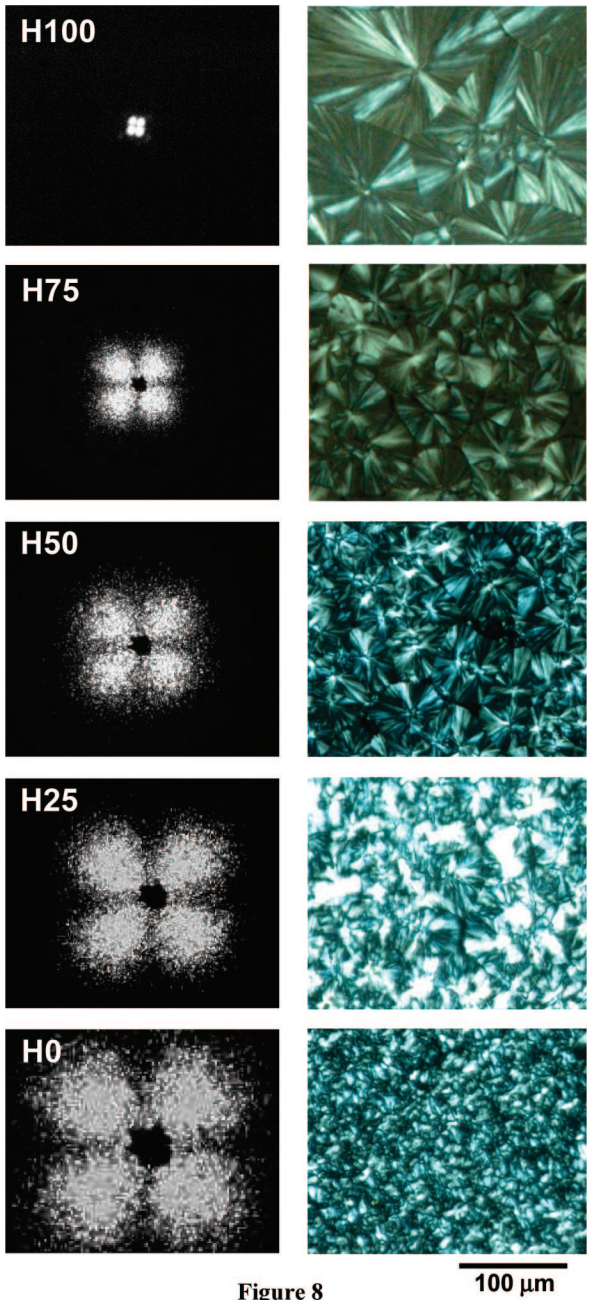

Figure 8. Polarized optical microscopic pictures and small-angle light scattering HV patterns taken for the H/D blends of iPP crystallized at the same $\Delta T = 57$ °C.

form the statistically mixed aggregation state. As a result, we might not have a crystal lattice in which the D and H chain stems are statistically randomly distributed. This type of speculation may not be applied to the case of iPP H/D blends as being judged from the continuous change in the crystallization rate depending on the D/H content. As will be reported elsewhere, we performed the time-resolved measurements of infrared spectra in the isothermal crystallization and found that the D and H chains crystallize at almost same timing, meaning the cocrystallization occurs with the H and D chains stems included together from the early stage. In other words, the H chains with originally slower crystallization rate are enhanced to crystallize by blending with the D chains, and inversely the crystallization rate of D chains is reduced to some extent depending on the D/H content.

As is well-known, in cases of miscible blend samples between the crystallizable and noncrystallizable polymer species, the

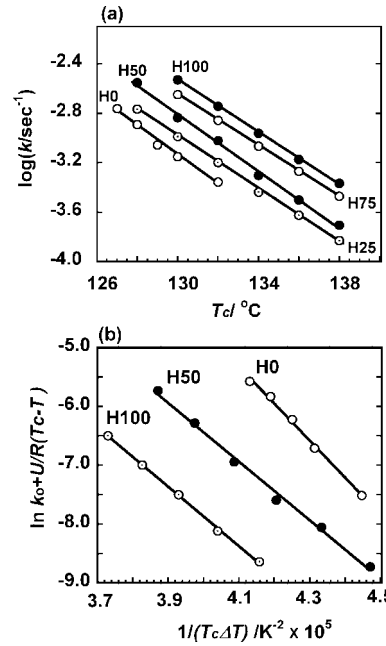

Figure 9. (a) H content dependence of log k estimated for a series of iPP H/D blend samples. (b) A Hoffman−Lauritzen plot for the H/D blends of iPP.

Table 3. Equilibrium Melting Temperatures, K_g, and k_0 Values for a Series of D/H Blend Samples

samples	$T°_m$/°C	$K_g \times 10^5$/K^{-2}	ln k_0
H100	196.5	6.9835	12.26
H75	194.6	3.6393	10.08
H50	192.3	4.8458	13.48
H25	189.2	4.1603	16.85
H0	187.5	4.5559	20.49

growth rate of spherulite radius is dependent on the blend ratio of these two components: the growth rate becomes lower as the noncrystallizable component is larger in population.[57,58] If the noncrystallizable species stays at the interface between the lamellar and molten regions, the growth rate is controlled by the relative diffusion rate of the two kinds of polymer chains: the lower diffusion of noncrystallizable polymer component results in the slower growth rate since the crystallizable polymer chains cannot approach the interface. Besides, the growth rate of the spherulite radius is proportional to the square rood of time.[59] Figure 12 shows the growing behaviors of spherulite radius estimated for H50 and H100 samples, which were obtained by performing the time-dependent measurement of isothermally induced spherulite growth under a polarized optical microscope. The growth rate is almost constant in the experimental time region, opposite the above-mentioned crystallizable/noncrystallizable blend sample case. Therefore, it might be said

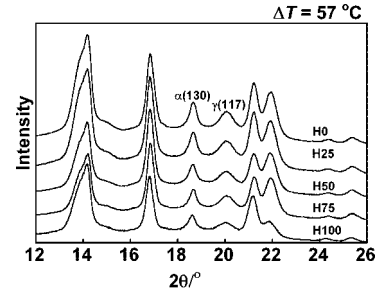

Figure 10. Wide-angle X-ray diffraction profiles measured for a series of H/D blend samples of iPP after isothermally crystallized at the same degree of supercooling ($\Delta T = 57$ °C).

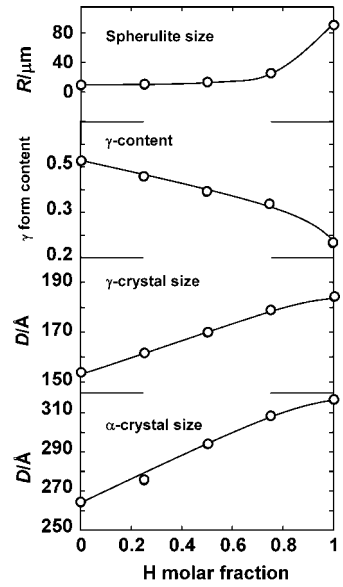

Figure 11. H content dependence of the spherulite size, content of the γ-form, the crystallite size of the γ-form, and the crystallite size of the α-form estimated for a series of iPP H/D blend samples.

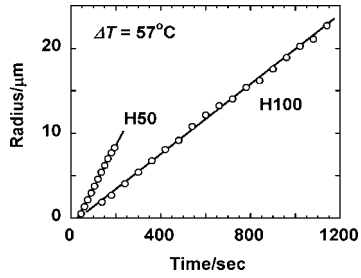

Figure 12. Time dependence of spherulite radius measured for H50 and H100 iPP D/H blend samples in the isothermal crystallization process at the same supercooling condition. The case of H0 is not shown here since the growing rate was too high to estimate the radius quantitatively accurately.

reasonably that the D and H species of iPP can migrate together by adjusting the diffusion rate in the melt, and they can approach the front part of the growing lamella at the same timing as mentioned above. In order to judge the correct situation of the crystallization behavior of the D/H blend samples of iPP including such a concept of diffusion motions of chains, the measurements of small-angle neutron scattering and infrared spectra of the molten state as well as the crystalline region may be helpful, which would be performed in the near future.

Concerning the crystallization rate k, the D species shows a higher k value than that of the H species. As shown in eq 5, the k is governed by the factors U and K_g. The U is related to the energy of transportation of chains and should be lower for the D chains with heavier mass. The lower U gives the higher k value. The K_g is related to the surface energies and ΔH°_m, which may be common to the D and H species. The molecular dynamics calculation might be helpful for furthermore interpretation of the different behaviors of the iPP D and H chain species.

Conclusion

In the present work, we studied the effect of isotope on the isothermal crystallization behavior of iPP for the first time. We found that the H/D blend sample with higher D content shows a higher crystallization rate when compared for the same ΔT. This difference results in the difference in such a morphology as spherulite shape, crystallite size, relative content of the α- and γ-forms, etc. It should be pointed out here that such a difference in crystallization rate of the pure H and D species is smaller for the D/H blend sample, where the cocrystallization occurs with almost random distribution of the H and D chain stems in the crystallites, indicating the migration rate of individual chain, for example, may be modified more or less in the coexisting state of the H and D chains in the melt.

Acknowledgment. This study was financially supported by a MEXT "Collaboration with Local Communities" project (2005−2009).

References and Notes

(1) A special issue on crystallization of polymers: *Faraday Discuss. Chem. Soc.* **1979**, *68*.
(2) *Proceedings of the NATO Advanced Research Workshops on Crystallization Process of Polymers*, Series C; Dasiere, M., Ed.; Kluwer Academic: Dordrecht, The Netherlands, 1993; Vol. *405*.
(3) Tasumi, M.; Krimm, S. *J. Chem. Phys.* **1967**, *46*, 755.
(4) Tasumi, M.; Krimm, S. *J. Polym. Sci., Part A-2* **1968**, *6*, 995.
(5) Krimm, S.; Ching, J. H. C. *Macromolecules* **1972**, *5*, 209.
(6) Stehling, F. C.; Ergos, E.; Mandelkern, L. *Macromolecules* **1971**, *4*, 672.
(7) Mitsuhiro, S.; Stein, R. S.; Han, C. C. *Macromolecules* **1985**, *18*, 2179.
(8) Takeno, H.; Koizumi, S.; Hasegawa, H.; Hashimoto, T. *Macromolecules* **1996**, *29*, 2440.
(9) (a) Coutry, S.; Spells, S. J. *Polymer* **2002**, *43*, 4957. (b) Coutry, S.; Spells, S. J. *Polymer* **2003**, *44*, 1949. (c) Coutry, S.; Spells, S. J. *Polymer* **2006**, *47*, 3410.
(10) Tashiro, K.; Stein, R. S.; Hsu, S. L. *Macromolecules* **1992**, *25*, 1801.
(11) Tashiro, K.; Satkowski, M. M.; Stein, R. S.; Li, Y.; Chu, B.; Hsu, S. L. *Macromolecules* **1992**, *25*, 1809.
(12) Tashiro, K.; Izuchi, M.; Kobayashi, M.; Stein, R. S. *Macromolecules* **1994**, *27*, 1221.
(13) Tashiro, K.; Izuchi, M.; Kobayashi, M.; Stein, R. S. *Macromolecules* **1994**, *27*, 1228.
(14) Tashiro, K.; Izuchi, M.; Kobayashi, M.; Stein, R. S. *Macromolecules* **1994**, *27*, 1234.
(15) Tashiro, K.; Izuchi, M.; Kaneuchi, F.; Jin, C.; Kobayashi, M.; Stein, R. S. *Macromolecules* **1994**, *27*, 1240.
(16) Sasaki, S.; Tashiro, K.; Gose, N.; Imanishi, K.; Izuchi, M.; Kobayashi, M.; Imai, M.; Ohashi, M.; Yasuo, Y.; Ohayama, K. *Polym. J.* **1999**, *31*, 677.
(17) (a) Shelten, J.; Wignall, G. D.; Ballard, D. G. H. *Polymer* **1974**, *15*, 682. (b) Shelten, J.; Ballard, D. G. H.; Wignall, G. D.; Longman, G. W.; Schmatz, W. *Polymer* **1976**, *17*, 751. (c) Shelten, J.; Ballard, D. G. H.; Wignall, G. D.; Longman, G. W.; Schmatz, W. *Colloid Polym. Sci.* **1974**, *252*, 749. (d) Shelten, J.; Wignall, G. D.; Ballard, D. G. H.; Longman, G. W. *Polymer* **1977**, *18*, 1111.
(18) Yoon, D. Y.; Flory, P. J. *Macromolecules* **1976**, *9*, 294.
(19) (a) Alamo, R. G.; Londono, J. D.; Mandelkern, L.; Stehling, F. C.; Wignall, G. D. *Macromolecules* **1994**, *27*, 411. (b) Wignall, G. D.; Londono, J. D.; Alamo, R. G.; Lin, J. S.; Galante, M. J.; Mandelkern, L. *Macromolecules* **1995**, *28*, 3156.
(20) Men, Y.; Rieger, J.; Lindner, P.; Enderle, H. F.; Lilge, D.; Kristen, M. O.; Mihan, S.; Jiang, S. *J. Phys. Chem. B* **2005**, *109*, 16650.
(21) Ryan, A. J.; Fairclough, J. P. A.; Terrill, N. J.; Olmsted, P. D.; Poon, W. C. K. *Faraday Discuss.* **1999**, *112*, 13.
(22) Iijima, M.; Strobl, G. *Macromolecules* **2000**, *33*, 5204.
(23) Heeley, E. L.; Maidens, A. V.; Olmsted, P. D.; Bras, W.; Dolbnya, I. P.; Fairclough, J. P. A.; Terrill, N. J.; Ryan, A. J. *Macromolecules* **2003**, *36*, 3656.
(24) Li, L.; De Jeu, W. H. *Phys. Rev. Lett.* **2004**, *92*, 75506.
(25) Natta, G.; Corradini, P. *Nuovo Cimento Suppl.* **1960**, *15*, 40.
(26) Brückner, S.; Meille, S. V.; Petraccone, V.; Pirozzi, B. *Prog. Polym. Sci.* **1991**, *16*, 361.
(27) Janimak, J. J.; Cheng, S. Z. D. *Polym. Bull.* **1989**, *22*, 95.
(28) Hoffman, J. D.; Davis, G. T.; Lauritzen, J. I., Jr. Crystalline and Noncrystalline Solids In *Treatise on Solid State Chemistry*; Hannay, N. B., Ed.; Plenum Press: New York, 1976; Vol. *3*, p 497.
(29) Clark, E. J.; Hoffman, J. D. *Macromolecules* **1984**, *17*, 878.
(30) Martuscelli, E.; Pracella, M.; Crispino, L. *Polymer* **1983**, *24*, 693.
(31) Maiti, P.; Hikasoka, M.; Yamada, K.; Toda, A.; Gu, F. *Macromolecules* **2000**, *33*, 9069.
(32) Fatou, J. M. G.; Barrales-Lienda, J. M. *J. Polym. Sci., Part A-2* **1969**, *7*, 175.
(33) Blundell, D. J.; Beckett, D. R.; Willcocks, P. H. *Polymer* **1981**, *22*, 704.

(34) Fichera, A.; Zanneti, R. *Makromol. Chem.* **1975**, *176*, 1885.
(35) Brückner, S.; Meille, S. V.; Petraccone, V.; Pirozzi, B. *Prog. Polym. Sci.* **1991**, *16*, 361.
(36) Ballard, D. G. H.; Cheshire, P.; Longman, G. W.; Schelten, J. *Polymer* **1978**, *19*, 379.
(37) Ballard, D. G. H.; Longman, G. W.; Cowley, T. L.; Cunningham, A.; Schelten, J. *Polymer* **1979**, *20*, 399.
(38) Ballard, D. G. H.; Burgess, A. N.; Nevin, A.; Cheshire, P.; Longman, G. W.; Schelten, J. *Macromolecules* **1980**, *13*, 677.
(39) Reddy, K. R.; Tashiro, K.; Sakurai, T.; Yamaguchi, N. *Macromolecules* **2008**, *41*, 9807.
(40) Stein, R. S.; Rhodes, M. B. *J. Appl. Phys.* **1960**, *31*, 1873.
(41) Champion, J. V.; Killey, A.; Meeten, G. H. *J. Polym. Sci., Polym. Phys. Ed.* **1985**, *23*, 1467.
(42) *Polymer Handbook*; Brandrup, J., Immergut, E. H., Grulke, E. A., Eds.; John Wiley & Sons: Hoboken, NJ, 1999; Vol. *2*.
(43) Hoffman, J. D.; Weeks, J. J. *J. Res. Natl. Bur. Stand.* **1962**, *66*, 13.
(44) Mezghani, K.; Philiphs, P. J. *Macromolecules* **1994**, *27*, 6145.
(45) Avrami, M. J. *J. Chem. Phys.* **1939**, *7*, 1103.
(46) Avrami, M. J. *J. Chem. Phys.* **1940**, *8*, 212.
(47) Avrami, M. J. *J. Chem. Phys.* **1941**, *9*, 177.
(48) Wunderlich, B. *Macromolecular Physics*; Academic Press: New York, 1976; Vol. *2*, p 115.
(49) Godoviskii, Y. K. *Polym. Sci. USSR* **1969**, *11*, 1462.
(50) Chen, J. H.; Yao, B. X.; Su, W. B.; Yang, Y. B. *Polymer* **2007**, *48*, 1756.
(51) Alwattari, A. A.; Lloyd, D. R. *Polymer* **1998**, *39*, 1129.
(52) Korshak, V. V.; Kozyreva, N. M.; Skubina, S. B.; D'yachkovskii, F. S.; Tsvetkova, V. I.; Nedorezova, P. M. *Polym. Sci. USSR* **1981**, *23*, 3027.
(53) Wang, Y. F.; Lloyd, D. R. *Polymer* **1993**, *34*, 4740.
(54) Fischer, D.; Mulhaupt, R. *Macromol. Chem. Phys.* **1994**, *195*, 1433.
(55) Perez, E.; Zucchi, D.; Sacchi, M. C.; Forlini, F.; Bello, A. *Polymer* **1998**, *40*, 675.
(56) Alamo, R. G.; Kim, M. H.; Galante, M. J.; Isasi, J. R.; Mandelkern, L. *Macromolecules* **1999**, *32*, 4050.
(57) Turner-Jones, A. *Polymer* **1971**, *12*, 487.
(58) Bragatto, G.; Gianotti, G. *Eur. Polym. J.* **1983**, *19*, 803.
(59) Schultz, J. M. *Polymer Crystallization*; Oxford University Press: New York, 2001.

MA802568C